J Mol Model (2008) 14:607–620
DOI 10.1007/s00894-008-0319-7

ORIGINAL PAPER

Mesoscopic simulation studies on micellar phases of Pluronic P103 solution

Shouhong Yang · Xiuqing Zhang · Shiling Yuan

Received: 8 December 2007 / Accepted: 16 April 2008 / Published online: 14 May 2008

Abstract The microphase separation dynamics of the triblock copolymer surfactant P103 [(ethylene oxide)$_{17}$ (propylene oxide)$_{60}$(ethylene oxide)$_{17}$] was investigated by a dynamic variant of mean-field density functional theory. Different self-assembled aggregates, spherical micelles, micellar clusters and disk-like micelles, are explored in the solution. The spherical micelle above critical micelle concentration (CMC) is a dense core consisting mainly of PPO and a hydrated PEO swollen corona, and is in good agreement with the experimental results concerning their structures. At a concentration of 10–15%, micellar clusters with a larger PPO core form as a result of coalescence among spherical micelles. At concentrations above 16% by volume, a series of disk-like micelles come into being. The order parameters show that spherical micelles are easily formed, while the micellar clusters or disk-like micelles need a longer time to reach steady equilibrium. The results show that mesoscopic simulation can augment experimental results on amphiphilic polymers, and provide some mesoscopic information at the mesoscale level.

Keywords Mesoscopic simulation · Micelle · Pluronics

Introduction

Pluronics, also termed Poloxamers or Synperonics, are block PEO-PPO-PEO copolymers of poly(ethylene oxide) (PEO) and poly(propylene oxide) (PPO). In aqueous solution, these block copolymers behave like surfactant molecules and can build a wide variety of aggregates as a consequence of their amphiphilic character. Under appropriate conditions, they can form multimolecular micellar, bicontinuous, hexagonal and lamellar phases. The properties of Pluronic aggregates have been extensively investigated via many techniques such as microcalorimetry [1–3], small-angle neutron or X-ray scattering [4–7], static [8] and dynamic [9, 10] light scattering, and rheometry [11–14]. In such studies, spherical micelles, in which a hydrophobic block is gathered into a spherical core and the hydrophilic block is solvated by water, are typical. Experimental investigations on different aggregates are helpful in understanding the structures and properties of a Pluronics solution [15, 16].

In the past decade, computer simulation methods have proven to be valuable tools in studies of the phase behavior of polymers. All-atomic molecular dynamics (MD) simulation approaches permit modeling of morphological evolution in polymeric systems during phase separation. Furthermore, mesoscopic simulation methods, such as dissipative particle dynamics (DPD) [17, 18] and self-consistent field theory (SCFT) [19–21], are promising simulation approaches that have been widely accepted. These latter methods treat the polymeric chains in a coarse-grained (or mesoscopic) level by grouping atoms together, which can be extended to several orders of magnitude in length and time scales as compared to all-atomic MD simulations [22, 23]. The SCFT method is basically a self-consistent field approximation with "plugged in" phenomenological density dynamics, and it does not take into account polymer chain dynamics, hydrodynamic interactions, etc. Compared with conventional particle simulation

S. Yang · X. Zhang · S. Yuan (✉)
Key Laboratory of Colloid and Interface Chemistry,
Shandong University,
Jinan 250100, People's Republic of China
e-mail: shilingyuan@sdu.edu.cn

methods, field-based methods like SCFT have relatively high computational efficiency. This has led to significant advances in the investigation of the microphase separation of block copolymers [24–28].

Using SCFT simulations, we recently investigated the phase behaviors of Pluronic P65 under shear [29] and discussed the effect of a weakly charged block on the lamellar phase of Pluronic P85 [30]. In present study, the same SCFT method is used to investigate the phase behavior of Pluronic P103 in aqueous solution. Figure 1 shows the different micellar phases of P103 solution at low concentration, i.e., spherical micelle, micellar cluster and disk-like micelle. In fact, at high concentrations (above 45% vol, see the supporting information), bicontinuous and lamellar phases are also found. In this paper, we focus only on morphologies found at low concentration (below 20% vol). In Fig. 1 it can be seen that spherical micelles form only at concentrations from 4 to 9% vol, and their sizes are around 3.5 nm; micellar clusters of more than 5.0 nm are formed by the coalescence of different spherical micelles form at concentrations of 10–15% vol; disk-like micelles form above 16% vol.

The paper is arranged as follows: first, approaches to the transition Gaussian chain and the interaction parameters used in SCFT are elaborated, and the background of the method is simply described; then, different morphologies are shown via the 3D density fields; finally, the effect of temperature on the spherical micelles is discussed.

Methods and model

The basic idea of the SCFT method is that the free energy, F, of an inhomogeneous liquid is a function of the local density function, ρ, from which all thermodynamic functions can be derived. The SCFT model consists of various types of beads, I, J, …, with interactions described by harmonic oscillator potentials for the intramolecular interactions [31]. Each bead is a certain component type representing covalently bonded groups of atoms such as those given by one or a few structural units of a polymer chain. The dynamics of such a system is described by a set of functional Langevin equations. These represent diffusion equations in the component densities, which take account of the noise in the system.

On a coarse-grained time scale, $\rho_I^0(\mathbf{r})$ is defined as a collective concentration field of type I beads at an instant in time and serves as a reference level. There will be a certain distribution of bead positions, defined as $\psi(\mathbf{R}_{11},\ldots,\mathbf{R}_{nN})$, where $\mathbf{R}_{\lambda s}$ is the position of bead s from chain λ. Given the distribution ψ, the collective concentration of bead s from all chains can be defined by the average of a microscopic density operator:

$$\rho_I[\psi](\mathbf{r}) \equiv \sum_{r=1}^{n}\sum_{s=1}^{N}\delta_{Is}^{K}\mathrm{Tr}\psi\delta(\mathbf{r}-\mathbf{R}_{\lambda s}) \quad (1)$$

(δ_{Is}^K is the Kronecker function with value 1 when bead s is of type I and 0 otherwise). It is assumed that, in a liquid

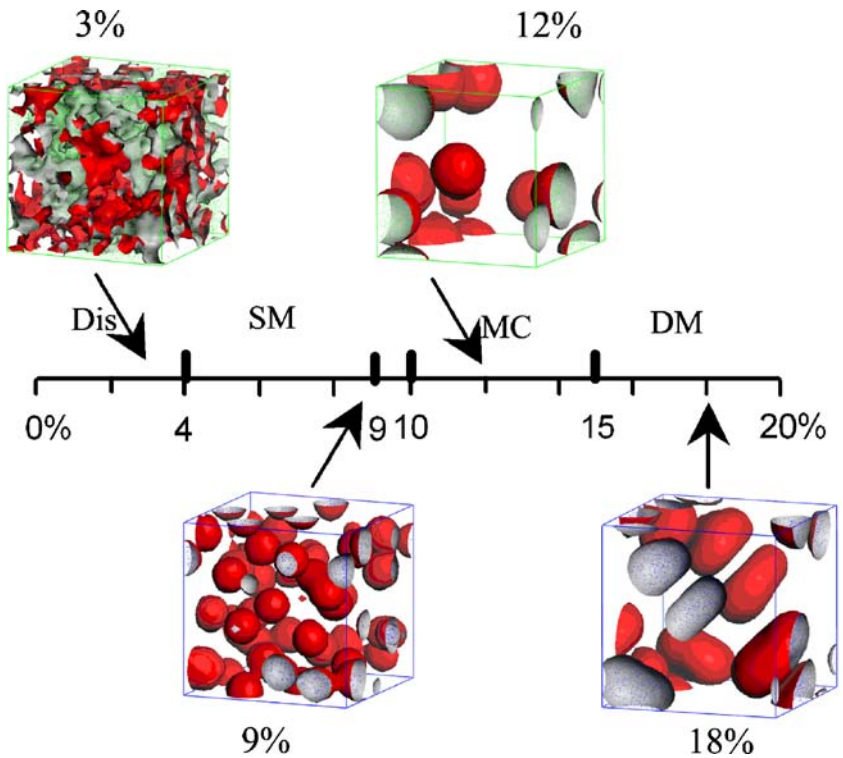

Fig. 1 Simulated phase diagram of Pluronic polymer in aqueous solution at 298 K. Phases are labeled as *Dis* (disorder), *SM* (spherical micelle), *MC* (micellar cluster), *DM* (disk-like micelle)

with high viscosity (slowly relaxation), the interactions do not depend on the momenta. A set of distribution functions ψ is defined with the constraint $\rho_I^0(\mathbf{r}) = \rho_I[\psi](\mathbf{r})$. All distributions ψ belonging to the same density $\rho_I^0(\mathbf{r})$ form an equivalence class, Ω, of distribution functions:

$$\Omega = \left\{\psi(\mathbf{R}_{11}, \ldots, \mathbf{R}_{nN}) | \rho_I[\psi](\mathbf{r}) = \rho_I^0(\mathbf{r})\right\} \tag{2}$$

On the basis of this set of distribution functions, an intrinsic free-energy functional $F[\psi]$ can be defined:

$$F[\psi] = \mathrm{Tr}\left(\psi H^{id} + \beta^{-1}\psi \ln \psi\right) + F^{nid}\left[\rho^0\right] \tag{3}$$

The first term is the average value of the Hamiltonian for internal Gaussian chain interactions [32]. The second term in the free-energy functional represents the entropy of the distribution $-k_B T\psi \ln\psi$. The third term is the mean-field nonideal contribution. ψ is independent of the history of the system, and is fully characterized by the constraint (on the density distribution that minimizes the free-energy function). This constraint is realized by means of an external potential U_I.

The constraint minimization of the free-energy functional leads to an optimal distribution, which can be written in terms of densities and external potential as:

$$F[\rho] = -\beta^{-1} n \ln \Phi + \beta^{-1} \ln n! - \sum_I \int U_I(\mathbf{r})\rho_I(\mathbf{r}) d\mathbf{r} + F^{nid}[\rho] \tag{4}$$

Φ is partition function of the chain. Now the model for the nonideal free-energy functional is introduced,

$$F^{nid}[\rho] = \frac{1}{2} \times \iint \begin{bmatrix} \varepsilon_{AA}(|\mathbf{r}-\mathbf{r}'|)\rho_A(\mathbf{r})\rho_A(\mathbf{r}') + \varepsilon_{AB}(|\mathbf{r}-\mathbf{r}'|)\rho_A(\mathbf{r})\rho_B(\mathbf{r}') \\ +\varepsilon_{BA}(|\mathbf{r}-\mathbf{r}'|)\rho_B(\mathbf{r})\rho_A(\mathbf{r}') + \varepsilon_{BB}(|\mathbf{r}-\mathbf{r}'|)\rho_B(\mathbf{r})\rho_B(\mathbf{r}') \end{bmatrix} d\mathbf{r}d\mathbf{r}' \tag{5}$$

where $\varepsilon_{IJ}(|\mathbf{r}-\mathbf{r}'|)$ is a mean-field energetic interaction between beads of type I at r and type J at r′.

The mean-field intrinsic chemical potential can easily be derived via functional differentiation of the free energy: $\mu_I(\mathbf{r}) = \delta F/\delta\rho_I(\mathbf{r})$. At equilibrium, $\mu_I(r)$= constant, which results in the familiar self-consistent-field equations for the mean-field Gaussian chain model. In general, these equations have many solutions, corresponding to stable or metastable states; the one with the lowest free energy is of particular interest. On the basis of these equations, the generalized time-dependent Ginzburg-Landau theory can be set up [32]

$$\frac{\partial\rho_A(\mathbf{r})}{\partial t} = Mv\nabla\cdot\rho_A\rho_B\nabla[\mu_A - \mu_B] + \eta \tag{6}$$

$$\frac{\partial\rho_B(\mathbf{r})}{\partial t} = Mv\nabla\cdot\rho_A\rho_B\nabla[\mu_B - \mu_A] + \eta \tag{7}$$

The distribution of the Gaussian noise η satisfies the fluctuation-dissipation theorem:

$$\langle\eta(\mathbf{r},\mathbf{t})\rangle = 0 \tag{8}$$

$$\langle\eta(\mathbf{r},\mathbf{t})\eta(\mathbf{r}',\mathbf{t}')\rangle = -\frac{2Mv}{\beta}\delta(t-t')\times\nabla_{\mathbf{r}}\cdot\delta(\mathbf{r}-\mathbf{r}')\rho_A\rho_B\nabla_{\mathbf{r}'} \tag{9}$$

where M is a bead mobility parameter. The kinetic coefficient $Mv\rho_A\rho_B$ models a local exchange mechanism. The Langevin equations are constructed for an incompressible system with dynamic constraint:

$$\rho_A(\mathbf{r},t) + \rho_B(\mathbf{r},t) = \frac{1}{v} \tag{10}$$

where v is the average bead volume.

To specify the chemical nature of the system, two sets of parameters must be defined: one is the chain topology in terms of repeat segments (or beads), and the other is the interaction energy of the various components. For the first set, the SCFT uses a Gaussian chain "spring and beads" description, in which all segments are of the same size, and the chain topology depends on the coarsened degree of the original system. In this model, springs mimic the stretching behavior of a chain fragment, and different kinds of beads correspond to different components in the block co-polymer. Lam [33] described the relationship between atomistic chains and Gaussian chains of block polymers using the Monte Carlo method. The Gaussian bond length is

$$a \approx \frac{X}{x}L_{PEO} \approx \frac{Y}{y}L_{PPO} \tag{11}$$

L_{PEO} and L_{PPO} are the monomer sizes of EO and PO, respectively, estimated by assuming an all-trans conformation L_{PEO}=0.2910 nm and L_{PPO}=0.3394 nm [33]. X and Y refer to the number of units in the PEO and PPO block polymer, respectively. x and y are the numbers of coarsened chain topology. van Vlimmeren [34] derived another simple relation for the atomistic and Gaussian chains:

$$\frac{X}{x} \approx 4.3, \quad \frac{Y}{y} \approx 3.3 \tag{12}$$

Since both x and y have to be integers, the above equations cannot be solved exactly. A few approximating values in each equation are shown for Pluronic P103 in Table 1. It is worth noting that these two approaches can give a similar Gaussian chain, $A_4B_{18}A_4$, where the

Table 1 Gaussian chain approximation for Pluronic P103

Real co-polymer chain	Methods	Calculated		Approximated		Gaussian chain
		x	*y*	*x*	*y*	
$PEO_{17}PPO_{60}PEO_{17}$	Lam [33]	4.3	17.6	4	18	$A_4B_{18}A_4$
	van Vlimmeren [34]	4.0	18.2	4	18	

solvophobic B beads represent PPO blocks and the solvophilic A beads are PEO blocks.

The interaction energies ε_{IJ} of the various types of segments represent the pairwise interactions of beads, similar to that defined in the Flory-Huggins model [33]. These can be derived either from atomistic simulation [33, 35], empirical methods [36] or from experimental data such as vapor pressure data [34]. The simplest approach is based on regular solution theory and relates the Flory-Huggins model to the component solubility parameter δ. These parameters can be considered as the nonideal interactions, and the strength of repulsion interaction between different components is characterized by $\varepsilon_{AB}>0$. In the calculations, the simulation parameters of P103 are $\chi_{AB}=3.0$, $\chi_{AS}=1.3$ and $\chi_{BS}=1.7$, reflecting the interaction strengths between two components A (slightly solvophilic), B (slightly solvophobic), and S (solvent), respectively. Of course, in the mean-field model, any polymer surfactant solution with the same properly scaled interaction parameters will behave in exactly the same way. These defined parameters are compared with experimental microphase diagrams of Pluronic aqueous solution for our work [28–30] or other studies [24–27, 33, 34]. The simulations will be stopped when the order parameters no longer change, which represents the characteristics of phase separation and the mean-squared deviation from homogeneity in the system.

Results and discussion

Morphology of the micellar phase

As shown in Fig. 1, three phases of the copolymer solution—spherical micelles, micellar clusters and disk-like micelles—are formed in low concentration (below 20% vol). In the following, the different morphologies will be discussed using 3D density fields, and the changes of the order parameters with time evolution are investigated.

Spherical micelles

As the copolymer concentration in water is higher than the critical micellar concentration (CMC), micelles start to form. In our simulation, the typical spherical micelles are formed at a concentration of 4–9% vol. In order to gain insight into phase separation, we carefully analyzed the

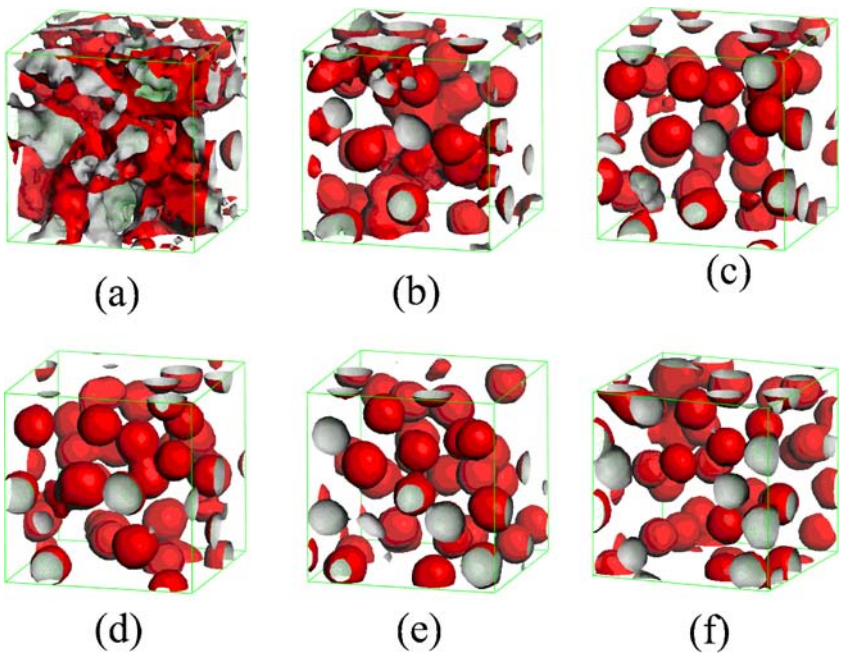

Fig. 2 The isosurface of density fields for spherical micelles in a 6% vol system with time evolution. **a** 0.125, **b** 0.25, **c** 0.375, **d** 0.5, **e** 1.0 and **f** 2.5 ms

typical micelles in a 6% vol system. Figure 2a–f shows the isosurface of solvophobic B with time evolution at 0.125, 0.25, 0.375, 0.5, 1.0 and 2.5 ms, respectively. These isosurfaces show that, to some extent, the solution is homogeneous at the beginning of simulation (Fig. 2a); raw micelles then come into being (Fig. 2b) and, finally, the solution arrives at equilibrium about 0.375 ms (Fig. 2c) and the typical spherical micelles are formed (several ms, Fig. 2e,f). These micelle dynamics show that the hydrophobic blocks in the solution can aggregate the cores, and it is easy to form spherical micelles in a short time (several hundred microseconds). With time evolution, these equilibriums can be maintained due to the complex interactions among the solvophilic block, solvophobic block, and solvent. In the simulation, the typical micelles do not coalesce together.

These dynamics can also be confirmed by time evolution of the order parameter (Fig. 3). The order parameter P is the mean-squared deviation from homogeneity in the system. It captures the effects of both phase separation and compressibility. Figure 3 indicates that the order parameter of the spherical micelle with time evolution can be divided into three stages [37]. In stage I, the order parameter increases slowly in the beginning of the homogeneous system, but without clear spherical micelles. This stage takes about 125 μs. Then, in stage II, spherical micelles are formed, and the order parameter rapidly increases in a short time (about 100 μs). In stage III, the system evolves slowly to overcome the defects formed in the earlier stage. This process is time-consuming, and the order parameter reaches equilibrium slowly. Since the volume fraction of solvent is 94%, the solvent aggregates more easily than the solvphobic B. Therefore, the order parameter of solvent is more than that of solvophobic B in the simulation, indicating that, in low concentration, the solvent is still the primary effector of the morphology of the system.

The numbers of spherical micelles formed are shown in Fig. 4 with time evolution. Many spherical micelles are formed in an 8 or 9% vol system in a short time, whereas fewer micelles are found in a 4% vol system even over a long evolution time. It is easy to understand that the solvophobic B in the solution aggregates among the hydrophobic cores more easily when the concentration is above the CMC. It is worth noting that the number of micelles barely changes when the system is in stage III, characterized by the order parameters discussed in Fig. 3, indicating that the system can reach equilibrium after a long simulation time.

The structures of spherical micelles can be drawn through the density field of different beads that represent the block polymer or solvent molecules. For demonstration, the 8% vol P103 system is considered. First, the best density slices of EO, PO and water along the x-axis of a cubic grid are created. Then, three slices are divided as shown in Fig. 5a. Here, the same spherical micelle is chosen in all three slices (shown by dotted lines in Fig. 5b). From these slices, the density distribution curves of different molecules (EO, PO and water) are obtained (illustrated in Fig. 5c). There are two small peaks in the density distribution of hydrophilic EO, a large peak for hydrophobic PO, and a trough for water molecules. From these features, we deduce the structure of spherical micelle (see Fig. 5d): the flexible PEO block disperses in water and forms the corona of the micelle, the PPO block is hydrophobic and forms the micellar core, with very few water molecules remaining in it. The segregation between the PPO and PEO block is not strong enough to cause a sharp boundary between micellar core and corona, and the

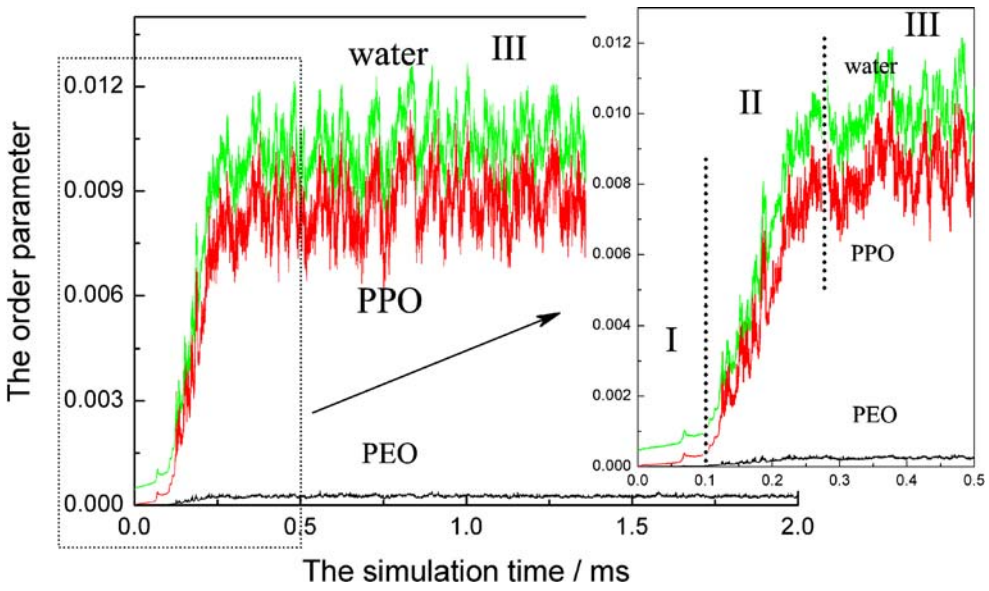

Fig. 3 Order parameter plot with increasing time for 6% vol P103. *Inset* Exploded view of the nucleation stage

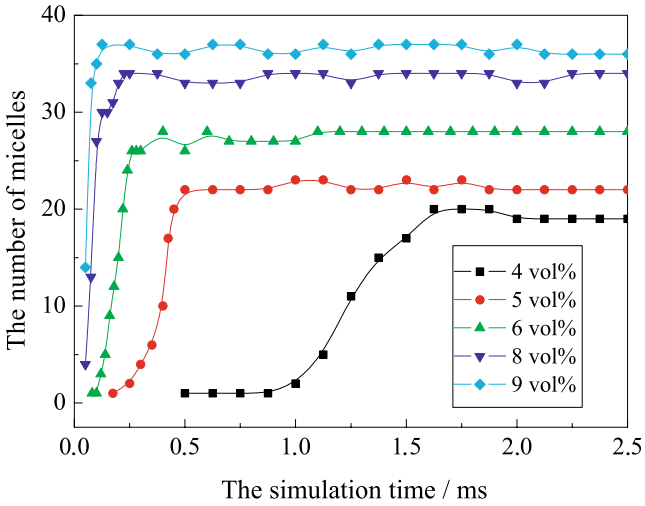

Fig. 4 The number of spherical micelles for P103 with time evolution

diffusive interface between core and corona characterises the spherical micelles formed by the Pluronic polymer. It should be noted that the structure of core and corona is unaffected by changes in Pluronic concentration. This result confirms the structure of spherical micelles proposed by experimental findings [38–41], i.e., a spherical micelle is composed of a central core of dense PPO with an outer corona of hydrated PEO units. It can be concluded that the simulation can provide much mesoscale information for block copolymers.

Micellar clusters

Although the order parameters of a 15% vol system have time evolution behavior similar to that of the spherical micelles system, the curve of the order parameter is divided

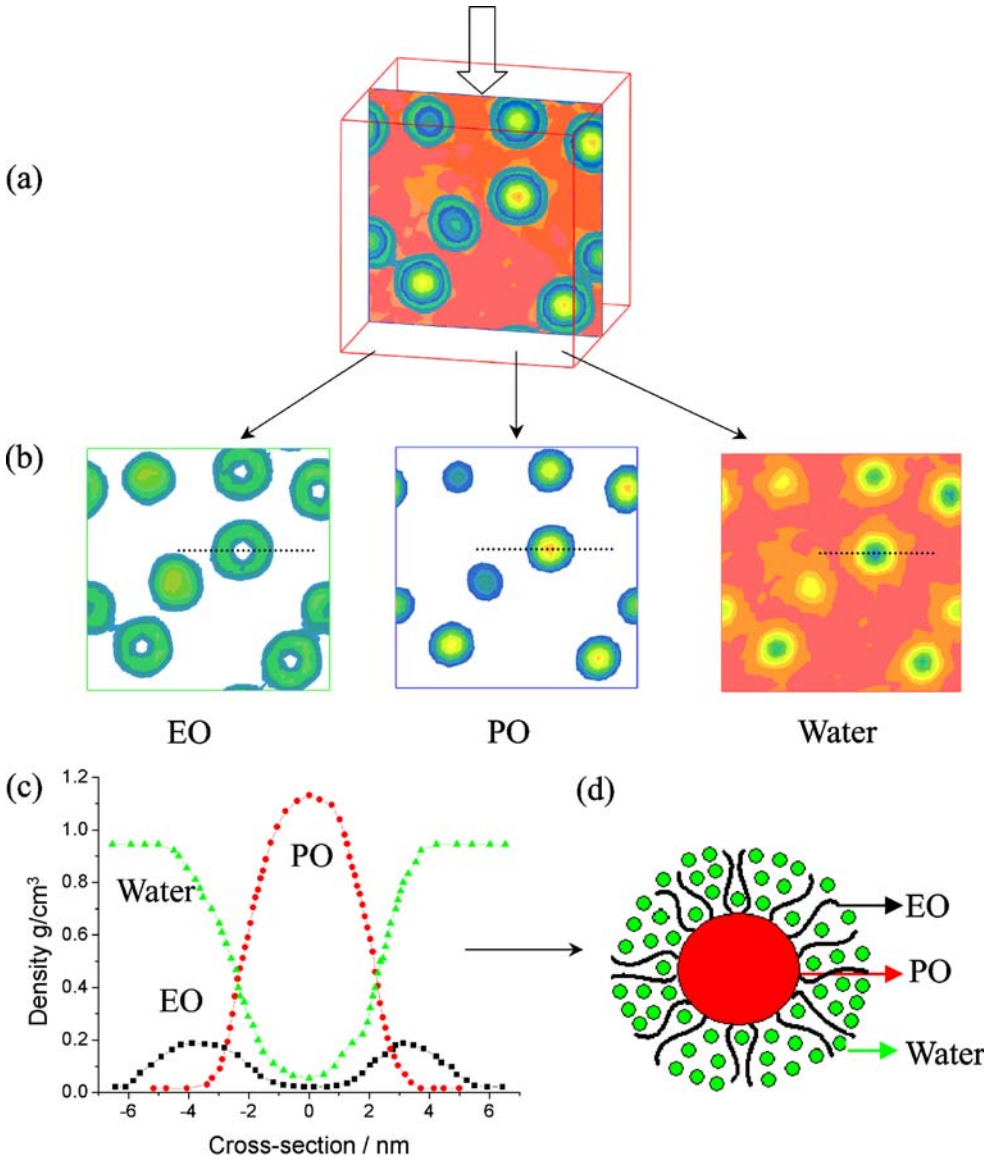

Fig. 5 Schematic structure of a spherical micelle. **a** Total slices of ethylene oxide (EO), propylene oxide (PO) and water molecules; **b** density slices of EO, PO and water, respectively; **c** density distributions of three compositions; **d** sketch structure of micelle. *Arrow* Position of slice in cubic cell

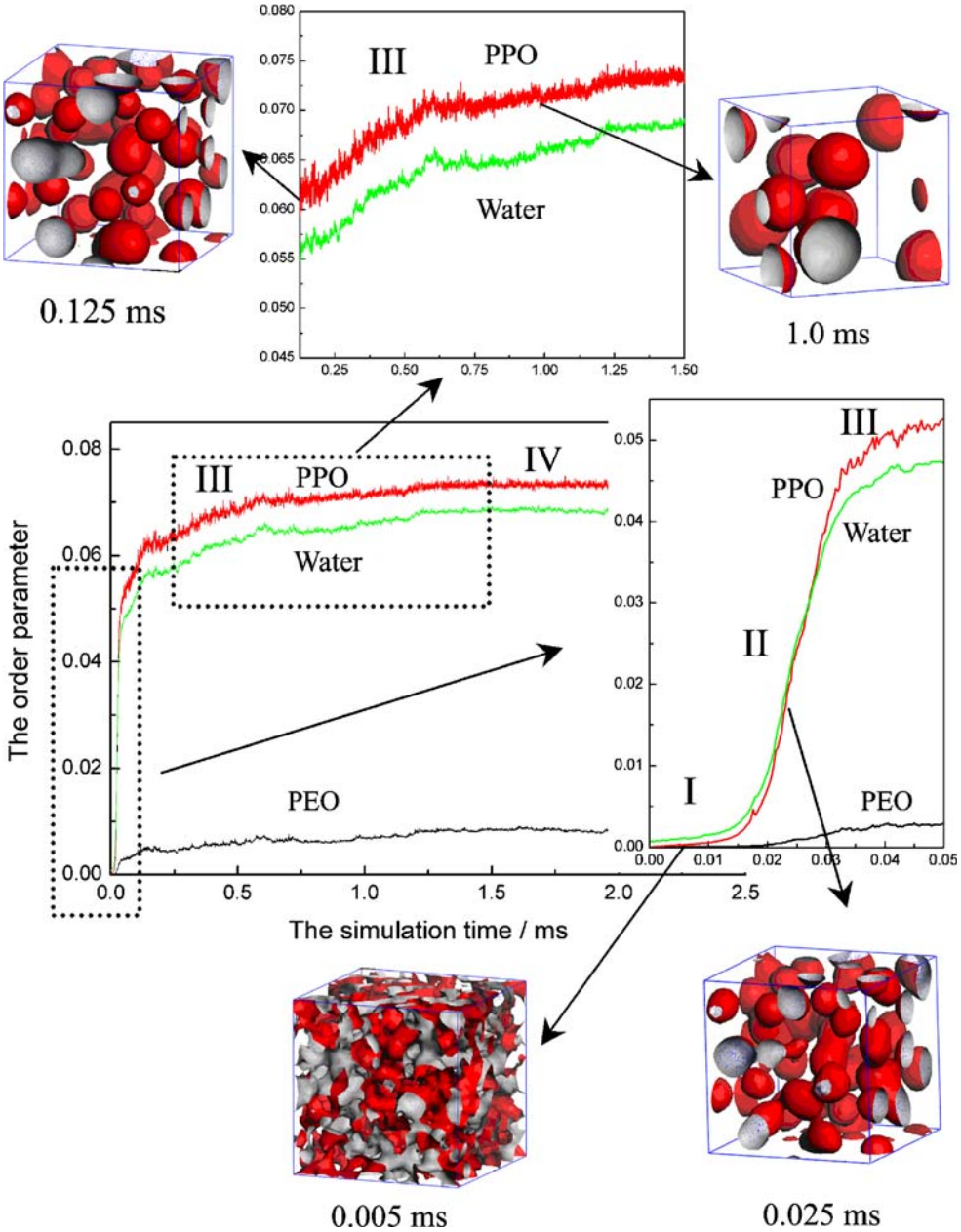

Fig. 6 Order parameter plot with time evolution for a 15% vol system. *Inset* Exploded view of nucleation stage

into four stages (Fig. 6) as far as the morphologies of the system are concerned. As shown in Fig. 6, in stages I and II the time evolution of the order parameters are similar to those in the 6% vol system (Fig. 3), i.e., the order parameter changes slowly from the starting homogeneous system, and then increase rapidly. In the 15% vol system, these two stages need a much shorter time than in the counterpart 6% vol system. Formation of micelles is expected to be easier at higher concentrations. Although the order parameters increase rapidly in stage II, the number of spherical micelles decreases slowly, and the duration of this stage is very short (about 15 μs).

In stage III, the order parameter resumes a slow increase with time evolution. Due to the coalescence of spherical micelles, many "big micelles" are formed in the solution. It is worth noting that the core sizes of these "big micelles" are larger than those of spherical micelles, with the difference between them being more than 2 nm. Herein, we refer to these "big micelles" as micellar clusters, to indicate that they result from coalescence of several spherical micelles. In fact, cluster formation was also reported by Brown et al. [42] in their dynamic light scattering experiments for Pluronic F87 and F88 in aqueous solutions. Our simulation confirms their findings that a Pluronic solution can form micellar clusters at an appropriate concentration. In the present simulation, micellar clusters form only at concentrations of 10–15% vol at 298 K. To further reveal the coalescence between spherical

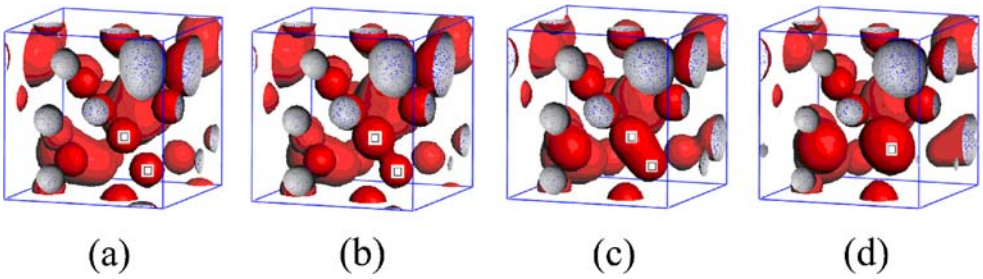

Fig. 7 Coalescence of micelles with time evolution for a 15% vol system. □ Spherical micelle that coalesce. **a** 180 μs, **b** 190 μs, **c** 225 μs, and **d** 250 μs

micelles, some 3D density fields showing the phase separation are shown in Fig. 7. It was noted that the two spherical micelles randomly selected were able to coalesce to form a big cluster in several tens of microseconds. The third stage lasts about several hundred microseconds up to 1 ms in different systems. Otherwise, as shown in Fig. 6, the order parameter of PO is more than that of the solvent with time evolution in the third stage. Obviously, the micellar clusters of PPO blocks become the primary determinant of the morphology of the system when the concentration is above the CMC.

When many micellar clusters have formed, the system enters the most time-consuming phase, stage IV, in order for the system to overcome the residue defects of morphology. In the present study, the simulation is run for up to 2.5 ms, and the results can be considered as stationary.

One of the primary characteristics of micelle structure is its size. Figure 8 shows the core radius, R_c, with time evolution. After spherical micelles start to form, their core radius increases continually until coalescence among spherical micelles ends. Coalescence finishes at about 1.1 ms for a 15% vol system, i.e., a longer time than that required for an 11% vol system (Fig. 8). Viscosity in copolymer solution is known to be directly related to the volume fraction occupied by spherical micelles [33]. Since the 15% vol system has more micelles, the solution has a higher volume fraction of micelles. Thus, coalescence among spherical micelles needs a longer completion time in higher volume fraction (or in a high viscosity system).

After the logarithmic plot of core size versus simulation steps is drawn (Fig. 8a,b), one interesting result is found. The 15% vol system is analyzed as an example. On the curve shown in Fig. 8a, one inflexion at 140 μs corresponds to the time at which the spherical micelles begin to coalesce (see Fig. 6). The logarithmic plot of core size with time evolution can be divided into two stages according to the different gradients. Considering the morphology formed in the solution, the enlargement of core size is coincident with the discussions about the second and third stages of order parameter in Fig. 6. In stage II, spherical micelles are

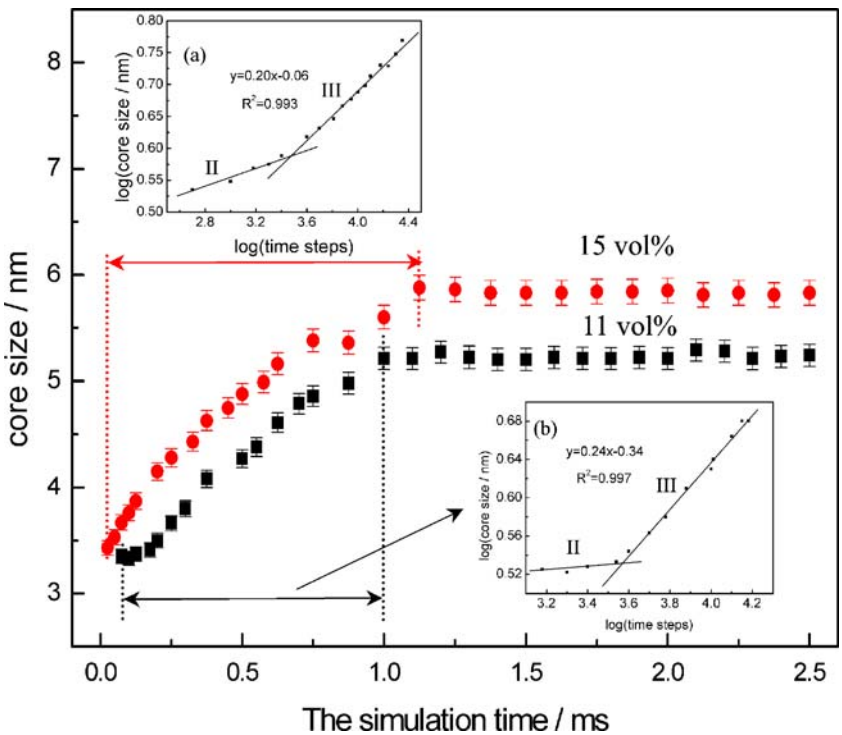

Fig. 8 Growth of core radius with time evolution for 11 and 15% vol systems. *Inset* Log–log plot of growth region

formed at the beginning. Then, in stage III, micellar clusters are formed due to coalescence of spherical micelles. According to the discussion above, a definition of four stages of order parameter with time evolution is reasonable in the micellar cluster phase.

Disk-like micelles

Above a concentration of 16% vol, another phase forms. As shown in Fig. 9, many disk-like aggregates in solution are observed in a 20% vol system. In the present paper, the morphology of this Pluronic solution is defined as disk-like micelle, which describes the oblate disk. The system needs several hundred microseconds to form these disk-like micelles. Mortensen [38] verified the oblate micelles in a solution of Pluronics P85 using small-angle neutron scattering, thus indicating that the disk-like micelles are not unique structures for the P103 system. In the simulation, it is difficult to distinguish micellar clusters from disk-like micelle phase only by depending on the data of the order parameter in equilibrium. However, like the order parameter of micellar clusters, the order parameter of disk-like micelles with time evolution is still divided into four stages. In Fig. 9, the morphology of hydrophobic B alters from small micelles to big disk-like micelles. Finally, many disk-like micelles are formed along one direction in the simulation cell. This results from the interaction between hydrophilic PEO blocks in neighboring disk-like micelles.

Throughout the simulations, it was noted that the disk-like micelles form at concentrations of 16–20% vol. When the concentration is above 20% vol, more complex morphologies are found, such as two phases regions, bicontinuous phases and lamellar phases (see the supporting information). In this paper, we focus on morphologies of Pluronics P103 at lower concentration (below 20% vol).

According to the simulations and discussions above, three types of micelles—spherical micelles, micellar clusters and disk-like micelles—are formed in P103 solution (below 20% vol). Figure 10 shows a schematic representation of these three micelles. In spherical micelle or micellar clusters (Fig. 10b,d), the hydrophobic PO blocks are gathered into spherical cores and the hydrophilic EO blocks are solvated by solvent. In disk-like micelles (Fig. 10e), EO blocks among different micelles twist together, and these micelles rearrange themselves in one direction.

Structural properties in different phases

As discussed above, core size is an important parameter of micellar structure. Figure 11a shows that the core size of the P103 system is a function of concentration for spherical micelles or in the micellar cluster phase. Since it is difficult to calculate the radius of these disk-like micelles, the phase of disk-like micelle in Fig. 11 is not concluded. It is easily divided into two parts from the data of the P103 system.

Initially, with increasing the concentration, the radius of spherical micelles decreases. At first glance, this may seem inconsistent with the increase in concentration. It is known from experiments that some water molecules are in the hydrophobic cores of the spherical micelle [43, 44], and our simulated structure also confirms this conclusion (see Fig. 5). Further investigation reveals that water molecules are extruded from the micellar cores with an increase in polymer concentration. Above the CMC, the hydrophobic

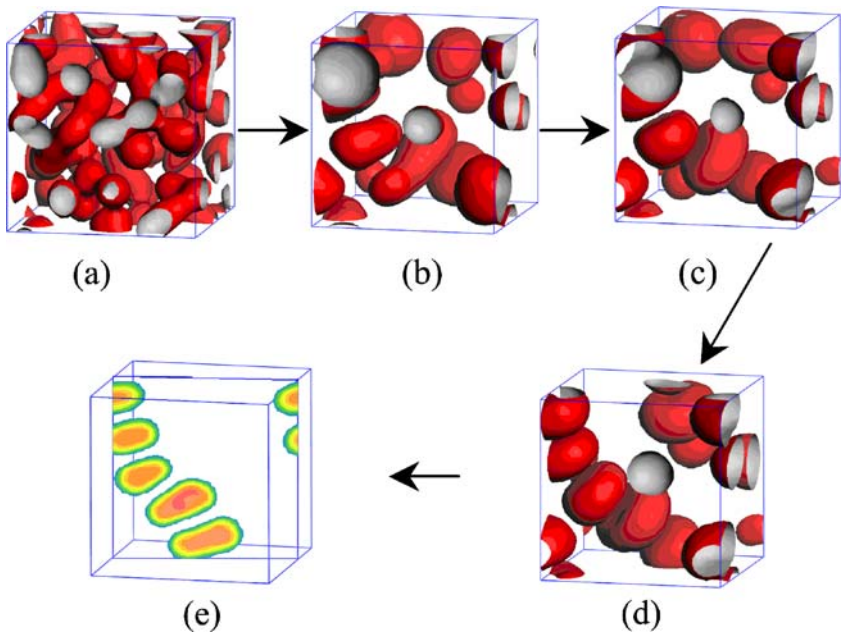

Fig. 9 The morphology with increasing time steps for a 20% vol system. **a** 15 μs, **b** 300 μs, **c** 500 μs, **d** 750 μs, **e** the best slice of 750 μs

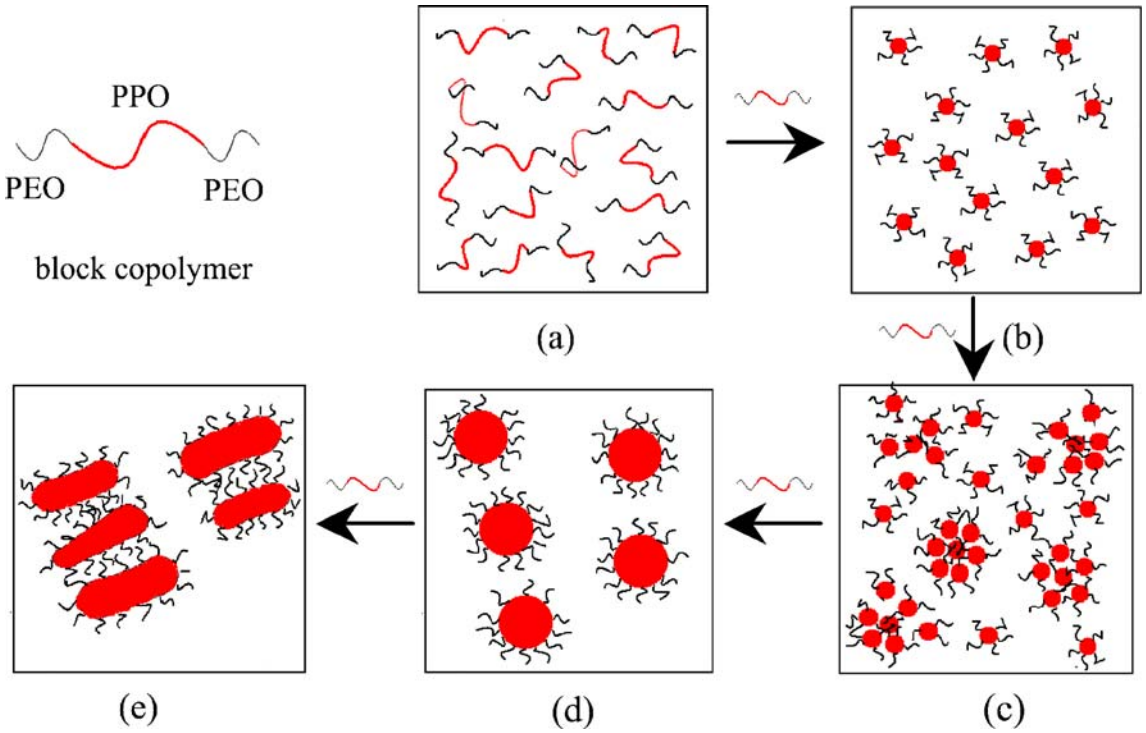

Fig. 10 Schematic representation of spherical micelles, micellar clusters and disk-like micelles of PEO-PPO-PEO types of block copolymers with increasing concentration. **a** Monomers in solution; **b** spherical micelles consisting of many copolymer molecules; **c** aggregates of independent hard-spheres; **d** micellar clusters due to coalescence of spherical micelles; **e** disk-like micelles

interaction becomes strong, and the coalescence of PPO blocks will extrude water molecules from the hydrophobic cores. Thus, the loose spherical micelles become dense spherical micelles, and the core size of the spherical micelles decreases. Another interesting phenomenon is that the core sizes of micelles in 7–9% vol are almost unchanged, indicating that "dry" spherical micelles have formed at these concentrations. When the concentration is above 9% vol, the radius of the "dry" micellar clusters increases rapidly. In this phase, the main driving force becomes coalescence of spherical micelles due to the hydrophobic interaction among PO blocks, and the additional PPO blocks will aggregate to form hydrophobic cores when the concentration is higher than the critical concentration of 9% vol of spherical micelles.

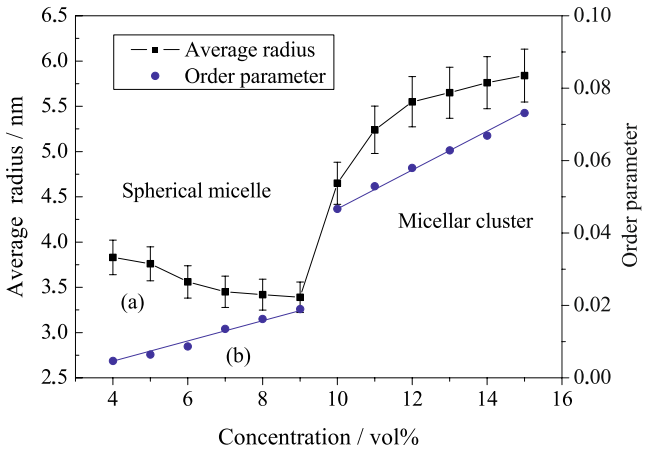

Fig. 11 Concentration dependence of core radius of micelles

The order parameters of different phase regions are shown in Fig. 11b. This can also be divided into two parts. Since the order parameter represents the characteristics of phase separation, the two stages of order parameter indicate that two obvious different phases are formed. According to the simulated morphologies, one is the phase of spherical

Table 2 Aggregation numbers of copolymer in micellar phases[a,b]

Concentration % vol	8	9	10	11	12	13	14	15
Aggregation number	29	28	74	104	125	130	140	146

[a] Since the spherical micelles formed in 6–7% vol are not "dry" micelles, the aggregation numbers of these system are not presented. In fact, several small spherical micelles are found in a 10% vol system along with micellar clusters. Thus, the average size of micelles in a 10% vol system is considered only as a reference number. The morphology of a 10% vol system at room temperature is shown in Fig. 14

[b] Since a system in low concentration (such as 4% vol or 6% vol) contains significant quantities of water, Eq. 6 cannot be used to calculate the aggregation number at lower concentration, thus aggregation numbers at lower concentrations are not exact. The aggregation number of 10% vol is considered as a reference average number, because there are several small spherical micelles in the solution

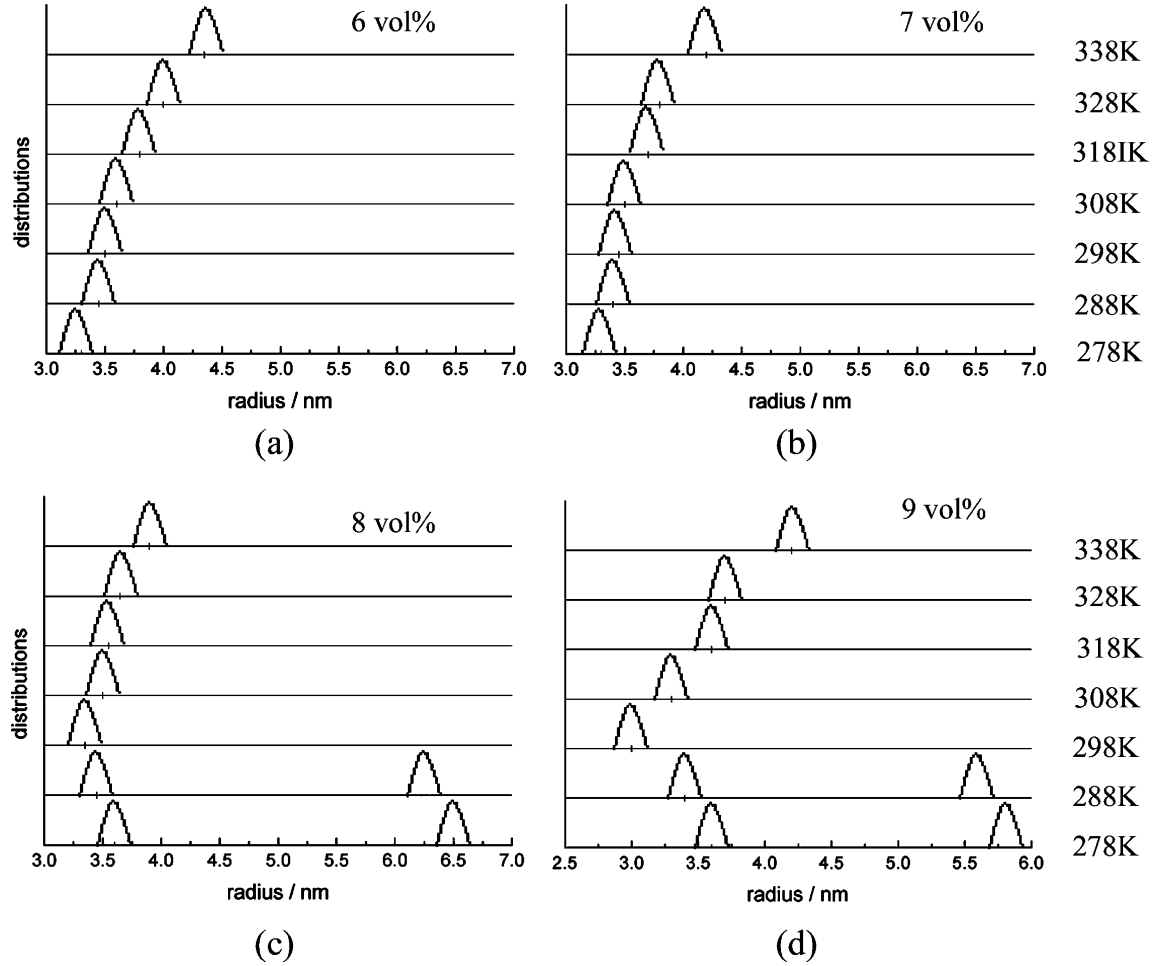

Fig. 12 The core sizes of micelles with increasing temperature. **a** 6% vol; **b** 7% vol; **c** 8% vol; **d** 9% vol

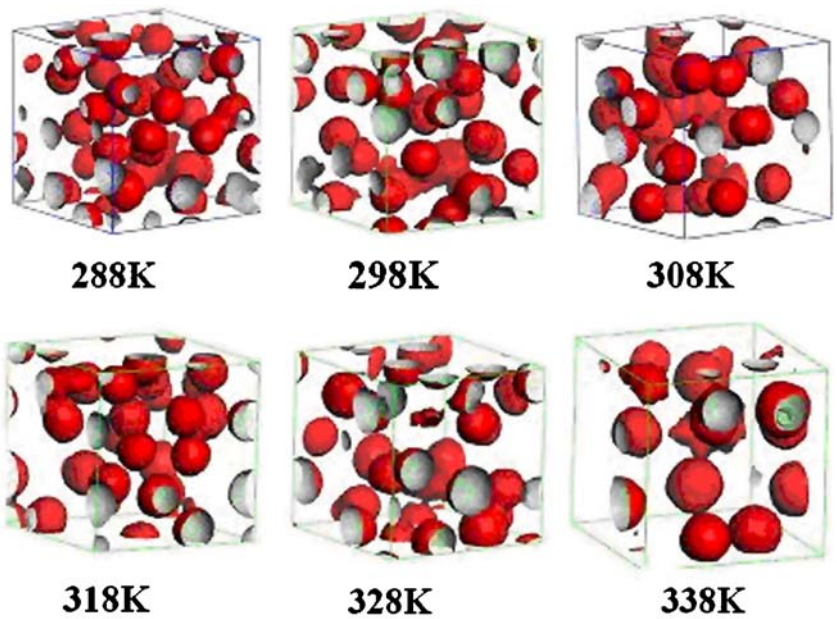

Fig. 13 Simulated morphology of a 6% vol system at 2.5 ms with increasing temperature

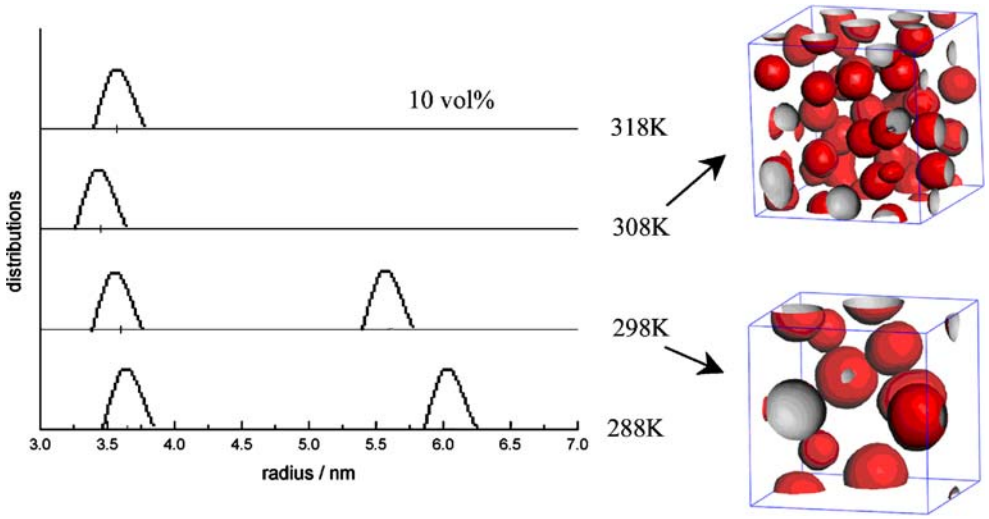

Fig. 14 Core sizes of micelles with increasing temperature for a 10% vol system

micelles, the other is the phase of micellar clusters. The two fitted lines of the different phases have different slopes, with that of the micellar cluster phase being steeper than that of the spherical micelle phase.

Another important parameter in Pluronic surfactant solution is the aggregation number. This can be independently calculated from knowledge of the core dimension. Assuming that the core consists only of PO—referred to as "dry" micelle in the discussion above—it is possible to derive the aggregation number (N) from the relationship [38]

$$4\pi R_c^3/3 = NYV_{PO} \tag{13}$$

where Y=60 is the number of units in the PO block polymer; and V_{PO}=95.4 Å^3 is the PO unit volume [45]. The aggregation numbers of different concentrations are listed in Table 2. An aggregation number of $N\approx28$ is found for a 9% vol system while $N\approx104$ for an 11% vol system at 298 K. Using a numerical self-consistent-field model, de Bruijn et al. [46] calculated N=58 for P103 solution. In fact, even when using the same technique, different authors report different aggregation numbers for the same Pluronics solution. For example, the aggregation numbers of Pluronic L64 are 88 at 315.5 K, 225 at 320.5 K [47], and 13 at 315 K, 50 at 318 K [48], calculated by different groups using the same light scattering experiments. We propose that our calculation of aggregate numbers provides another reference for experiment or simulation. In the simulation, the aggregation numbers of 10–15% vol concentrations are several times greater than those of 8–9% vol systems. Therefore, it is reasonable that the phase separations are divided into spherical micelles and micellar clusters in the discussion above.

The above discussion on changes of core size, aggregation numbers and order parameters with increases in concentration lead us to conclude that a 9% vol system can be considered as the boundary of spherical micellization. The system forms spherical micelles below 9% vol concentration, while it forms micellar clusters above 9% vol system. In spherical micelles, the hydrophobic PO forms a dense core containing little water, and water is extruded from the core with increasing copolymer concentration. However, when "dry" spherical micelles are formed, the core sizes of such micelles do not vary. If additional copolymers are added to the solution, larger cores of micellar clusters form due to the hydrophobic interactions of PPO. When the concentration is high enough, a string of disk-like micelles will be formed.

Influence of temperature on micelles

Temperature is known to have a profound effect on the phase separation of Pluronic copolymer in experiments due to its low critical solution behavior. Herein, we focus on the influence of temperature on spherical micelles. In this paper, we examine 6–9% vol systems, in which spherical micelles are formed at room temperature when equilibrium is achieved. As can be seen in Fig. 12, the core radius of spherical micelles in 6% vol system ranges from 3.3 nm at 278 K to 4.4 nm at 338 K. However, even at higher temperature (338 K), the core size of spherical micelles is

Table 3 Times required for phase separation

Temperature (K)	Time (μs)			
	6% vol	7% vol	8% vol	9% vol
288	82.2	50.7	37.2	28.8
298	120.9	56.8	41.8	32.5
308	136.7	74.4	49.7	40.8
318	219.2	103.1	71.5	53.5
328	487.2	182.6	92.3	65.7
338	1206.7	250.9	150.1	95.3

still smaller than that of micellar clusters, whose core sizes are more than 5.0 nm for 11–15% vol systems at 298 K (see Fig. 11). Therefore, we still define micelles as the spherical micelles formed at high temperature for 6–7% vol systems, not micellar clusters. The 3D density fields of the phase separation for a 6% vol system at different temperatures are shown in Fig. 13. Obviously, core size increases with increasing temperature. Linse et al. [49] used a spherical lattice model to calculate the core size of micelles of Pluronics, and found an increase in hydrodynamic radius with the increase of temperature. Our simulation confirms Linse's model.

For 8–9% vol systems (Fig. 12c,d) at low temperature (278 or 288 K), two types of micelle of different size are found together in solution. Since the difference in their core sizes is more than 2.0 nm, we define these as spherical micelles and micellar clusters. Alexandridis et al. [50] investigated the micelle size of P104 in solution using dynamic light scattering, and found that the polydispersivity of the micelle size decreases with temperature, i.e., the distribution of P104 micellar size is narrowed with increasing temperature. In our simulation for an 8–9% vol system (Fig. 12), large micelles diminish above 298 K, and only small spherical micelles with similar core sizes are found, indicating that micelles with the same radius are formed when the temperature is above a certain critical temperature; this finding is coincident with experimental results [50].

In a 10% vol system, since some spherical micelles with a 3.5–4.0 nm core size are found in solution and others have a core size above 5.5 nm, strictly speaking this system contains spherical micelles and micellar clusters together. Figure 14 shows the phase separation for a 10% vol system. At 308 K, the micellar clusters vanish, and many spherical micelles with the same core sizes form in the solution. These simulation results show that temperature has a strong impact on phase behavior of polymer solution. An increase in temperature enhances the hydrophobicity of PPO blocks, and the solubility of PEO and PPO in water decreases [51]. In contrast to PEO blocks, PPO blocks aggregate easily due to their high hydrophobicity in solution, and form cores easily at low temperature. Therefore, larger micellar clusters are found at low temperature, such as at 298 K for a 10% vol system and 288 K for 8–9% vol systems. From Table 3, it is worth noting that phase separation is more difficult and requires longer time at high temperature for each system, indicating that the hydrophobicity of the PO block is a very important factor determining the morphology of polymer solution and phase separation at different temperatures. As the temperature increases, the phase separation process slows down.

Since experimental investigation of the micro-morphology of Pluronic solution in low concentration is difficult, until now, other than de Bruijn's calculation [46] about the aggregate number in the solution, there has not been enough information about the micelle structure of P103 solution at the mesoscale level. Although experiments can give more information on macro-properties, simulations should be able to supply more mesoscale properties and structures. Our mesoscale simulation provides another method to investigate the morphology of Pluronic solution.

Summary

In this paper, the phase behaviors of Pluronic P103 solution were simulated using an SCFT method. The results show that, with increasing concentration of P123, the self-assembled aggregates progressively change from spherical micelles, micellar clusters, to disk-like micelles. In the spherical micellar region, the results of simulation resemble experimental results, in that they show that micelles comprise a dense core consisting mainly of PPO and a hydrated PEO swollen corona. Coalescence among spherical micelles forms larger micellar clusters. Due to the attraction between the PEO coronas of micellar clusters, a series of disk-like micelles are formed. The order parameters show that phase separation of spherical micelles is easily obtained, while micellar clusters or disk-like micelles need a longer time to reach steady equilibrium. As the temperature increases, micellar clusters vanish in solution, and phase separation becomes more difficult.

Acknowledgments This work was supported by the Young Science Foundation (2006BS04005) and Natural Science Foundation of Shandong Province (Y2007B09), China.

References

1. Alexandridis P, Holzwarth JF (1997) Langmuir 13(23):6074–6082
2. Michels B, Waton G, Zana R (2001) Colloids Surf A 183:55–65
3. Patterson I, Chowdhry B, Leharne S (1996) Colloids Surf A 111:213–222
4. Pedersen JK, Svaneborg C (2002) Curr Opin Colloid Interface Sci 7:158–166
5. King SM, Heenan RK, Cloke VM, Washington C (1997) Macromolecules 30:6215–6222
6. Eiser E, Molino F, Porte G, Diat O (2000) Phys Rev E 61:6759–6764
7. Liu Y, Chen SH, Huang JS (1998) Macromolecules 31:2236–2244
8. Liu Y, Chen SH, Huang JS (1998) Macromolecules 31:6226–6233
9. Jørgensen EB, Hvidt S, Brown W, Schillén K (1997) Macromolecules 30:2355–2364
10. Chen SH, Mallamace F, Faraone A, Gambadauro P, Lombardo D, Chen WR (2002) Eur Phys J E 9:283–286
11. Liu Y, Chen SH, Huang JS (1996) Phys Rev E 54:1698–1708
12. Chen ZR, Issaina AM, Kornfield JA, Smith SD, Grothaus JT, Satkowski MM (1997) Macromolecules 30(23):7096–7114
13. Schmidt G, Richtering W, Lindner P, Alexandridis P (1998) Macromolecules 31(7):2293–2298

14. Waton G, Michels B, Steyer A, Schosseler F (2004) Macromolecules 37(6):2313–2321
15. Lefèvre N, Fustin CA, Varshney SK, Gohy JF (2007) Polymer 48:2306–2311
16. Dimitrov P, Jamróz-Piegza M, Trzebicka B, Dworak A (2007) Polymer 48:1866–1874
17. Lahmar F, Rousseau B (2007) Polymer 48:3584–3592
18. Groot RD, Warren PB (1997) J Chem Phys 107:4423–4435
19. Fraaije JGEM (1993) J Chem Phys 99:9202–9212
20. Maurits NM, Altevogt P, Evers OA, Fraaije JGEM (1996) Comput Theor Polym Sci 6:1–21
21. Maurits NM, van Vlimmeren BAC, Fraaije JGEM (1997) Phys Rev E 56:816–825
22. Warren PB (1998) Curr Opin Colloid Interface Sci 3:620–624
23. Jawalkar SS, Adoor SG, Sairam M, Nadagouda MN, Aminabhavi TM (2005) J Phys Chem B 109(32):15611–15620
24. Maurits NM, Fraaije JGEM (1997) J Chem Phys 107:5879–5889
25. Fraaije JGEM, Sevink GJA (2003) Macromolecules 36(21): 7891–7893
26. Lyakhova KS, Zvelindovsky AV, Sevink GJA, Fraaije JGEM (2003) J Chem Phys 118:8456–8459
27. Altevogt P, Evers OA, Fraaije JGEM, Maurits NM, van Vlimmeren BAC (1999) J Mol Struct (THEOCHEM) 463:139–143
28. Li YM, Xu GY, Chen AM, Yuan SL, Cao XR (2005) J Phys Chem B 109:22290–22295
29. Zhang XQ, Yuan SL, Wu J (2006) Macromolecules 39(19): 6631–6642
30. Yuan SL, Zhang XQ, Xu GY, Zhang DJ (2006) J Mol Model 12:406–410
31. Bai GY, Nichifor M, Lopes A, Bastos M (2005) J Phys Chem B 109(1):518–525
32. Fraaije JGEM, van Vlimmeren BAC, Maurits NM, Postma M, Evers OA, Hoffman C, Altevogt P, Goldbeck-Wood G (1997) J Chem Phys 106:4260–4269
33. Lam YM, Goldbeck-Wook G (2003) Polymer 44:3593–3605
34. van Vlimmeren BAC, Maurits NM, Zvelindovsky AV, Sevink GJA, Fraaije JGEM (1999) Macromolecules 32:646–656
35. Zhang M, Choi P, Sundararaj U (2003) Polymer 44:1979–1986
36. Honeycutt JD (1998) Comput Theor Polym Sci 8:1–8
37. Guo SL, Hou TJ, Xu XJ (2002) J Phys Chem B 106(43):11397–11430
38. Mortensen K, Pedersen JS (1993) Macromolecules 26:805–812
39. Mortensen K, Brown W, Jorgensen E (1994) Macromolecules 27 (20):5654–5666
40. Linse P (1994) Macromolecules 27(10):2685–2693
41. Mortensen K, Brown W (1993) Macromolecules 26(16):4128–4135
42. Brown W, Schillen K, Hvidt S (1992) J Phys Chem 96:6038–6044
43. Su YL, Wang J, Liu HZ (2002) J Phys Chem B 106:11823–11828
44. Su YL, Wei XF, Liu HZ (2003) Langmuir 19:2995–3000
45. Karlstrom G (1985) J Phys Chem 89:4962–4964
46. de Bruijn VG, van den Broeke LJP, Leermakers FAM, Keurentjes JTF (2002) Langmuir 18(26):10467–10474
47. Zhou Z, Chu B (1988) J Colloid Interface Sci 126:171–180
48. Almgren M, Bahadur P, Jansson M, Li P, Brown W, Bahadur A (1992) J Colloid Interface Sci 151:157–165
49. Linse P, Malmsten M (1992) Macromolecules 25(20):5434–5439
50. Alexandridis P, Nivaggioli T, Alan Haton T (1995) Langmuir 11 (5):1468–1476
51. Horvat A, Lyakhova KS, Sevink GJA, Zvelindovsky AV, Magerle R (2004) J Chem Phys 120:1117–1126